MATERIALE PLASTICE
https://revmaterialeplastice.ro
https://doi.org/10.37358/Mat.Plast.1964

CC BY

Study on Bonded Performance of High-Strength Steel Wire Mesh with Polyurethane Cement: Analysis of Influencing Parameters

KEXIN ZHANG[1], JIAQI QIU[1], YI WANG[1], YIQI WANG[2]*
[1] School of Transportation and Surveying Engineering, Shenyang Jianzhu University, Shenyang, 110168, China
[2] College of Civil and Architectural Engineering, Heilongjiang Institute of Technology, Harbin, 150001, China

Abstract: *This paper proposes a new bridge reinforcement approach grounded in the technologically mature and extensively studied polymer mortar-HSSWM reinforcement technology. To verify the feasibility of this reinforcement method, this paper investigates the mechanical properties of high-strength steel wire mesh-polyurethane cement (HSSWM-PUC) composites through bond anchorage tests. The bond anchorage test of HSSWM with PUC was completed by setting wire diameter, longitudinal wire relative anchorage length, and transverse wire spacing as test variables. Some of the test results were verified by finite element analysis. The finite element model was established with the number of transverse wires, wire spacing, relative anchorage length, and wire diameter as variables. The experimental results were further studied and analyzed. The slip, ultimate load, and load-slip relationships of HSSWM and PUC under different variables were explored. Building upon this foundation, the variation rule between bond stress and slip of HSSWM-PUC composites is analyzed. Reducing the transverse wire spacing was found to increase the ability of the transverse wires to restrain the longitudinal wires. Meanwhile, with the increase of wire diameter, the bonding stress between HSSWM and PUC gradually decreases, whereas the bonding performance of PUC can be improved by appropriately reducing the ratio of adhesive powder.*

Keywords: *HSSWM, PUC, bonded anchorage test, finite element model*

1. Introduction

With socio-economic development, vehicle loads and flows have increased significantly [1]. Rapidly increasing vehicle loads, coupled with natural conditions such as acid rain, air, and temperature, cause reinforced concrete (RC) bridges to develop cracks, concrete deterioration, corrosion of reinforcing steel, and a multitude of other ailments. This eventually results in a decline in the bridge's load-bearing capacity, jeopardizing its long-term operation [2–4]. A large number of reinforced concrete structures have serious safety hazards and are in urgent need of repair and strengthening [5].

Commonly used bridge reinforcement methods include the paste reinforcement method, where the paste material is steel plate or carbon fiber plate [6]. The problem with the adhesive steel plate method is mainly in the connection between the plate and the existing bridge structure [7]. Due to the large area and stiffness of the steel plate, it is difficult to bond closely with the original structure. Coupled with the problems of self-weight and corrosion, the pasted steel plate is prone to fall off. While the method of pasting fiber cloth has the advantages of being lightweight and high strength. However, the carbon fiber material inherently exhibits properties of low shear strength, poor ductility, and uneven force, which need to be fully considered in the design [8–10]. When carbon fiber is used for bridge reinforcement, its aging cannot be ignored [11]. Improper surface preparation of carbon fiber cloth during construction may fail the plastering operation or detachment of the cement mortar layer [12].

*email: wangyiqihit@163.com

High-strength steel Wire Mesh (HSSWM) is lightweight and high-strength. Composite mortar is often used as the bonding and anchoring material, and HSSWM-composite mortar is used for bridge structure reinforcement [13–15]. An experimental study on the flexural performance of HSSWM-polymer mortar-reinforced concrete beams was carried out by Yuan et al. [16]. Findings from the study indicate that the application of this method can effectively inhibit the creation, formation, and development of cracks and reduce the width of cracks and the distance between cracks. Zhao et al. [17] studied the application of HSSWM-composite mortar for flexural performance reinforcement of reinforced concrete beams. When the number of longitudinal wires was 2, 4, and 6, the increase in the ultimate load capacity of the strengthened beams was 21.5%, 46.8%, and 60.9%, respectively. However, the poor tensile properties and bonding of the composite mortar led to the peeling and destruction of the HSSWM-composite mortar reinforcement layer, reducing the utilization rate of the HSSWM.

Polyurethane Cement (PUC) materials not only set quickly and have high early strength, but also exhibit the advantages of lightweight, high strength, and high toughness after curing. The material itself has good bond strength and resistance to acid and alkali corrosion [18]. However, when PUC is used alone to reinforce RC members, to more effectively enhance the load-bearing capacity of the members, the thickness of the PUC reinforcement layer is larger and the cost of the project is higher. In this paper, HSSWM is used as a reinforcing material and PUC is used as a matrix material to form a new type of reinforcing material, hereafter referred to as HSSWM-PUC. Both can give full play to the excellent mechanical properties of PUC and HSSWM, as well as exhibit a good economy [19,20].

HSSWM-PUC material, being a new composite material, the bonding and anchoring properties of HSSWM and PUC are the basis for the two materials to synergistically function. Meanwhile, the factors affecting the bonding properties of the two and the bond-slip model also need to be investigated. At present, scholars at home and abroad mainly conduct studies on influencing factors such as the type of rebar or wire, the corrosion rate of rebar or wire, and the strength grade of concrete or cement. To investigate the bond relationship between HSSWM and PUC, prismatic specimens of 15 specimen sets were fabricated in this paper. Pull-out tests were conducted with wire diameter, relative anchorage length, and transverse wire spacing as variables. At the same time, a finite element model is established to verify some of the experimental results. The experimental results are further investigated in depth by changing the model parameters. The damage characteristics and damage modes of the wire after pulling out from the PUC were determined, and a bond-slip model affecting the mechanical relationship between the wire and the PUC was proposed.

2. Materials and methods

2.1. Materials

2.1.1 PUC

PUC is made of cement and PUC emulsion uniformly mixed according to a certain proportion, the specific ratio is shown in Table 1. Polyurethane emulsions include isocyanates and polyester polyols. As a filler for PUC, the raw materials need to be dried in an oven for 2 h before use, to remove the free water in the raw materials. In addition, molecular sieves with a mass fraction of 10% need to be added in the preparation of PUC, to adsorb the water that cannot be removed from the raw material.

Table 1. Mass mixing ratios of PUC

Material	Percent
Isocyanate	25%
Polyester polyol	25%
Concrete	40%
Molecular sieve	10%

Polyurethane materials have good adhesion and chemical resistance. Two-component polyurethane is used as the polyurethane precursor, comprising isocyanate (black) and polyether polyol (white). The isocyanate (black material) and polyether polyol (white material) are shown in Figure 1. Isocyanate is a compound containing isocyanate (NCO), serving as one of the main raw materials for polyurethane materials. Polyether polyols, one of the main raw materials for polyurethane materials, are polymers formed through the linkage of ether bonds. Polyether polyols have good elasticity and ductility and are widely used in the production of elastomers, adhesives, sealants, and waterproof materials. Polyurethane materials can be generated by reacting with isocyanate. The material composition and chemical properties of the isocyanate and polyether polyol are shown in Tables 2 and 3.

Figure 1. Isocyanates (black material) and polyether polyols (white material)

Table 2. Composition of isocyanates

Substance name	Isocyanate	Diphenylmethane-44,4-diisocyanate
Composition	50%~70%	30%~50%

Table 3. Composition of polyether polyols

Substance name	Polyether polyol	Fluids	Epoxy catalyst
Composition	86%~89%	1%~4%	10%

2.1.2 PUC mechanical property

(1) PUC compression resistance

The PUC compressive test block size is 70 mm × 70 mm × 70 mm cube. Three compressive test blocks need to be poured incidentally into the casting of the PUC, and the cubic compressive strength test will be carried out according to the specification after the curing is completed. The mean compressive strength of the PUC used was measured to be 69.6 MPa.

(2) PUC flexural property

The size of the PUC flexural specimen is 100 mm × 100 mm × 400 mm rectangular. Again, three flexural specimens were cast incidental to the pour and tested for rectangular flexural strength according to the specification. The mean flexural strength was measured to be 47.6 MPa and the bending and tensile modulus of elasticity was 5000 MPa.

(3) PUC tensile strength

The PUC tensile specimens are dumbbell-type sheet specimens. Before testing, strain gauges are arranged symmetrically at the center of the specimen surface along the tensile direction. The average value of PUC tensile strength was determined as 33.8 MPa and the tensile modulus of elasticity was 4600 MPa.

2.1.3 High strength steel wire

Four sizes of stainless steel wires with diameters of 2.0, 2.4, 3.2, and 4.5 mm produced by Beijing Rongdaxin New Technology Co. were used in the test, as shown in Figure 2. Stainless steel wired wire consists of multiple steel wires wired together with a galvanized surface, a section structure configured as 7 × 7, and a tensile strength rating that varies according to the diameter. The mechanical property parameters of the steel wire are shown in Table 4.

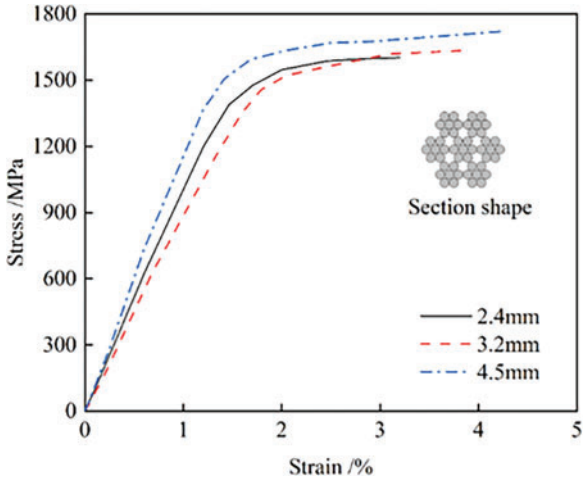

Figure 2. Stress-strain test curve of high-strength stainless steel wires

Table 4. Mechanical performance parameters of steel wires

Nominal diameter/mm	Ultimate load/kN	Ultimate tensile strength/MPa	Modulus of elasticity/GPa	Ultimate tensile strain/%
2.4	4.71	1601.82	108.74	3.26
3.2	8.26	1674.43	102.61	3.81
4.5	16.59	1783.61	98.35	4.19

2.2. Specimen design and preparation

In the bond anchorage test, the external dimensions of the prismatic specimens were 120 mm × 50 mm × 50 mm. The specimens were cast in one piece using wooden formwork and their exact dimensions are shown in Figure 3. Two transverse wires and one longitudinal wire were prearranged inside the specimen. The longitudinal wires were centered and passed through the prismatic specimen from top to bottom. The transverse wire is fixed to the longitudinal wire through clamps and anchored in position at the end of the wooden formwork.

The non-bonded area of the longitudinal wire is covered with a PVC pipe of the corresponding diameter so that the longitudinal wire in the non-bonded area is completely isolated from the PUC. This allows the relative bond length of the wire to the PUC to be varied by controlling the length of the PVC pipe. At the same time, the longitudinal wire is not damaged by the fixture when it is clamped. Carbon fiber cloth was wrapped around the loaded end and the carbon fiber cloth and wire were bonded with epoxy resin adhesive. The relative anchorage length la is selected according to multiples of the wire diameter, and four types are set: 12 times the diameter, 15 times diameter, 18 times diameter, and 22 times diameter. Combining the above test variables, the bond anchorage test was set up with 5 specimen sets and an aggregate of 17 specimen groups. Each specimen set contains 3 specimens with the same parameters to minimize test errors. The PA set consists of 4 specimen sets that are uniform except for

the difference in the transverse wire spacing l_b. Employed to investigate the effect of transverse wire spacing on the bonding properties of the material. Set B consists of 3 specimen sets with different relative anchorage lengths of longitudinal wires. Used to investigate the effect of the relative anchorage length of longitudinal wires on the bonding properties of the material. The PC set and the PD set each contain 4 specimen sets, and based on the PB set, only the wire diameter d. is changed. Utilized to investigate the effect of wire diameter on the bonding properties of the material. The PE set contains 2 sets of specimens with altered PUC ratios. Used to examine the influence of PUC powder ratio on material properties. The detailed design parameters for each specimen group are shown in Table 5.

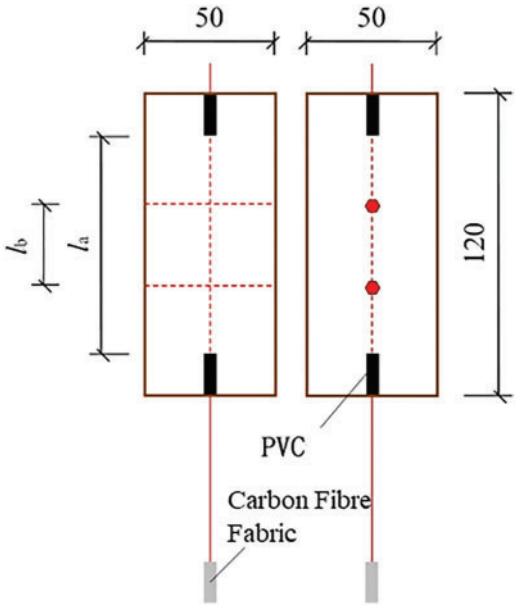

Figure 3. Dimensions of dumbbell prism specimens

The prismatic specimen is shown in Figure 4 and was fabricated as follows:

(1) Production and assembly of wooden formwork consisting of 1 base plate, 2 longitudinal side plates, and 2 short side plates. Glue the drilled holes in the side panels to the base plate and apply anti-seepage adhesive to the joints of the wooden formwork.

(2) Anchor the transverse and longitudinal wire ends to the side of the formwork with locking clasps, and use cross clasps to fix the HSSWM.

(3) Pour PUC into the wooden formwork and smooth the surface.

(4) After the specimens are poured, cling film is applied to seal the exposed cement surface. After 24 h, the formwork was removed and the specimens were placed in a standard curing chamber for curing. At the end of the incubation, the specimens were removed from the standard incubation room (temperature 20 ± 2°C) in preparation for the test.

Table 5. Design parameters of prism specimens

Specimen set	Specimen set	HSSWM diameter d/mm	Relative anchorage length of the longitudinal HSSWM network la/mm	Transverse HSSWM spacing lb/mm	PUC mixing ratio
PA	PA1	4.5	54 (12 d)	0	Match Ratio II
	PA2	4.5	54 (12 d)	20	Match Ratio II
	PA3	4.5	54 (12 d)	30	Match Ratio II
	PA4	4.5	54 (12 d)	40	Match Ratio II
PB	PB1	4.5	67.5 (15 d)	20	Match Ratio II
	PB2	4.5	81 (18 d)	20	Match Ratio II
	PB3	4.5	99 (22 d)	20	Match Ratio II
PC	PC1	3.2	38.4 (12 d)	20	Match Ratio II
	PC2	3.2	48 (15 d)	20	Match Ratio II
	PC3	3.2	64 (18 d)	20	Match Ratio II
	PC4	3.2	70.4 (22 d)	20	Match Ratio II
PD	PD1	2.4	28.8 (12 d)	20	Match Ratio II
	PD2	2.4	36 (15 d)	20	Match Ratio II
	PD3	2.4	43.2 (18 d)	20	Match Ratio II
	PD4	2.4	52.8 (22 d)	20	Match Ratio II
PE	PE1	4.5	81 (18 d)	20	Match Ratio I
	PE2	4.5	81 (18 d)	20	Match Ratio III

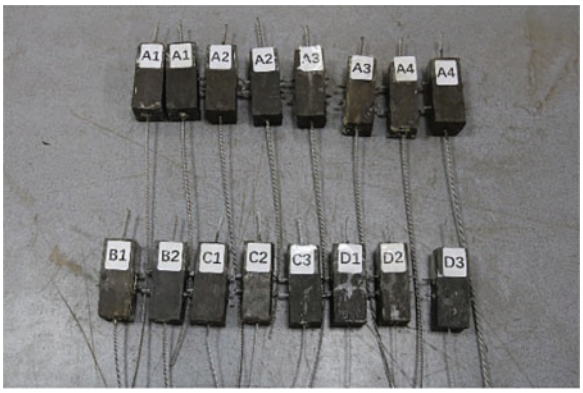

Figure 4. Manufactured prismatic specimens

2.3. Test set-up and measurement program

The bonding and anchoring tests were carried out on a WAW-50 kN microcomputer-controlled electro-hydraulic servo universal test machine. The loading device is shown in Figure 5. During the loading process, the lower fixture clamps the external steel wire and is fixed. The beam of the universal testing machine pulls the upper fixture upward, and the steel hanging basket pulls the prismatic specimen up together. The force sensor in the universal testing machine can collect the load in real-time. Three displacement meters are arranged on the upper surface of the PUC and the bottom of the steel hanging

basket. The slip of the lower end of the external steel wire can be measured by two displacement meters under the steel hoist basket. The displacement meter above the specimen can measure the slip of the upper end of the wire. Due to the fact that the steel wire and PUC inside the specimen will produce a certain length of deformation during the test. Therefore, the free end displacement minus the loading end displacement is the actual slip amount of the wire and PUC. The test is terminated when the following three conditions occur: (1) PUC splits and fails; (2) Steel wire fracture damage; (3) Slip failure of steel wire.

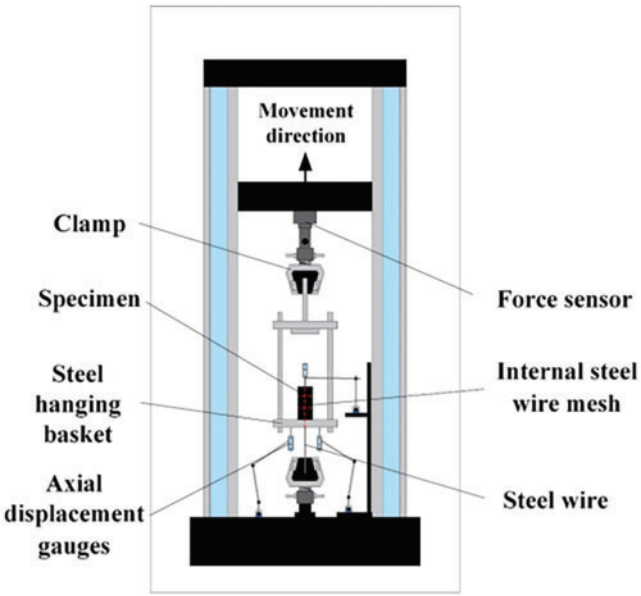

Figure 5. Test loading device

3. Results and discussions

3.1. Analysis of bonding and anchoring test results

3.1.1 PA specimen set bond anchorage test results

The test results for the PA set are shown in Table 6. The specimen sets belonging to the PA set had different transverse wire spacings and all experienced slip damage. In terms of ultimate load and maximum stress, there is little difference between the groups, with an average ultimate load of around 11 kN and an average maximum stress of around 14.5 kN. However, in terms of slip at ultimate load, the PA2 group with a transverse wire spacing of 20 mm had the smallest average slip of 1.06 mm. The PA4 group with a transverse wire spacing of 40 mm had the largest average slip of 1.39 mm. This shows that the transverse wire can constrain the longitudinal wire to some extent. This improves the ductility of the specimen during destruction and reduces the amount of slip. To verify the above experimental conclusions, a finite element model was established using ABAQUS, as shown in Figure 6. Due to the complexity of the wire surface, the wire was simplified in the modeling only to verify the experimental conclusions, as shown in Figure 7. The model was built using PA2 and PA4 specimen parameters and subsequently subjected to analysis. As shown in Figure 8, in the PA2 model, the ultimate load corresponds to a smaller slip of 1.20 mm. In the PA4 model, the slip corresponding to the ultimate load is larger at 1.48 mm. This is consistent with the above experimental findings, thus validating them. To further validate the above conclusions, finite element models were developed with transverse wire spacing of 20, 30, 40, and 60 mm, respectively. The relationship between the transverse wire spacing and the slip corresponding to the peak load was further verified. As shown in Figure 9, when the transverse wire spacing is 20, 30, 40, and 50 mm, the slip corresponding to the peak load is 1.20, 1.31, 1.48, and

1.83 mm, respectively. Slip corresponding to the peak load increases with the increase of the transverse wire spacing. The accuracy of the above experimental findings was further verified.

Table 6. Test results under set PA

Specimen set	Specimen set	Ultimate load Fu/kN	Maximum stress τu/MPa	Slip at ultimate load Su/mm	Type of damage
	PA1-1	11.21	14.69	1.19	Slip damage
PA1	PA1-2	11.09	14.54	1.08	Slip damage
	PA1-3	11.16	14.62	1.13	Slip damage
	PA2-1	11.05	14.48	1.05	Slip damage
PA2	PA2-2	11.00	14.41	1.02	Slip damage
	PA2-3	11.08	14.52	1.11	Slip damage
	PA3-1	11.13	14.59	1.20	Slip damage
PA3	PA3-2	11.02	14.44	1.25	Slip damage
	PA3-3	11.04	14.47	1.15	Slip damage
	PA4-1	11.09	14.53	1.41	Slip damage
PA4	PA4-2	11.13	14.59	1.44	Slip damage
	PA4-3	11.11	14.56	1.32	Slip damage

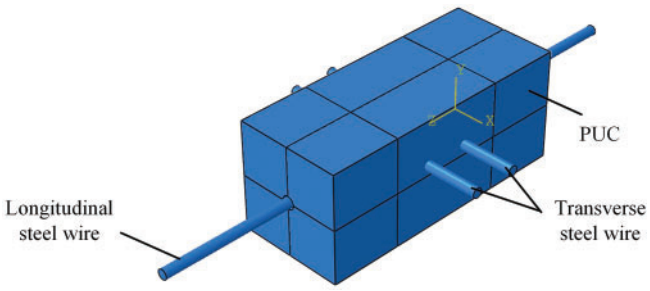

Figure 6. Finite element model of experimental specimen

To further explore the effect of the number of transverse wires on the slip corresponding to the peak load, finite element models were developed with the number of wires of 2, 3, and 4, respectively. The spacing of the transverse wires in the models was all 20 mm, and the models were analyzed separately. The simulation results are shown in Figure 10. When the number of transverse wires in the model is 2, 3, and 4, the slip corresponding to the peak load is 1.20, 1.05, and 0.99 mm, respectively. It can be seen that the greater the quantity of transverse wires in the modeled specimen, the smaller the slip corresponding to the peak load. This shows that the number of transverse wires also exerts a significant influence on the slip corresponding to the peak load.

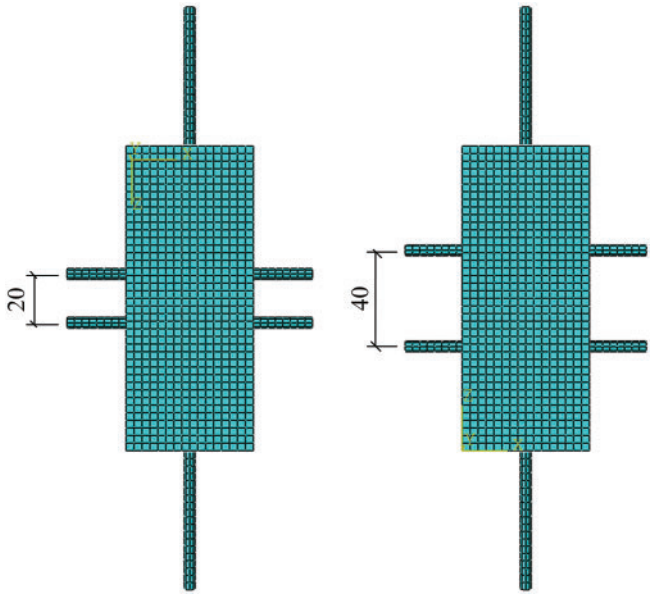

Figure 7. Finite element model of PA2 and PA4 specimens

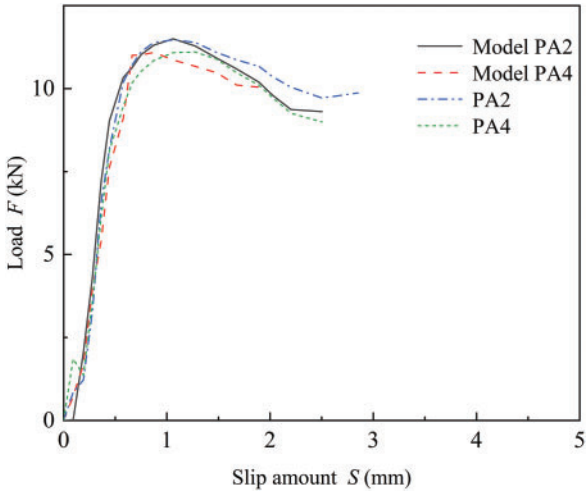

Figure 8. Model load-slip curves for PA2 and PA4 specimens

The PA specimen set load-slip relationship curve is shown in Figure 11. All four sets of specimens reached the ultimate load at a slip of about 1 mm. The PA1 group, due to the absence of transverse wires, showed a rapid decrease in load values after the ultimate load was reached until a maximum slip of 7.8 mm was reached. During the preloading period, all sets of curves maintained a high rate of increase. As the load continues to increase, the PA1 group is the first to reach the ultimate load. Since no transverse wire was configured in the PA1 group, its load-slip curve decreased rapidly after reaching the maximum load until it reached a maximum slip of 8 mm. While the load-slip curves of group PA2 (l_b = 20 mm), group PA3 (l_b = 30 mm) and group PA4 (l_b = 40 mm) dropped to 9 kN and started to oscillate after reaching the maximum load of 11 kN. The load was then eased to 2.5 kN and the specimen suffered slip damage.

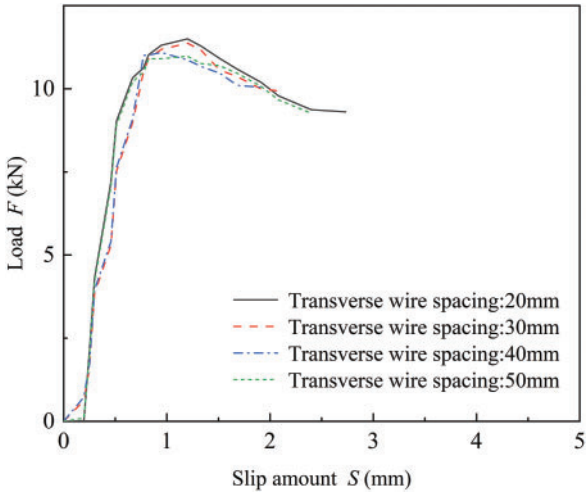

Figure 9. Load-slip curves for models with different transverse wire spacing

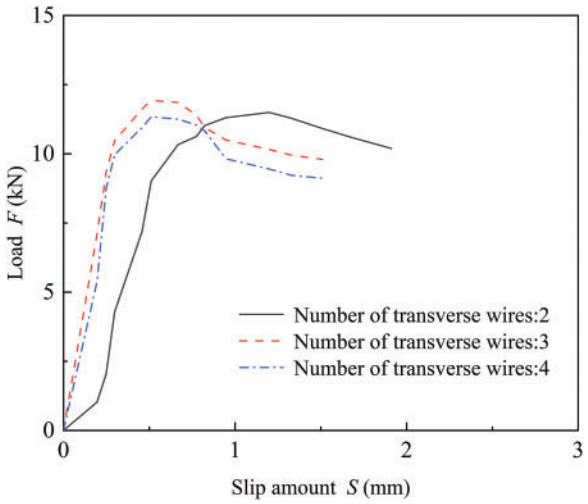

Figure 10. Load-slip curves for models with different numbers of transverse wires

3.1.2 PB specimen set bond anchorage test results

Table 7 lists the test results under the PB specimen set. The test variable for the PB set is the relative anchorage length of the longitudinal wire. Among the three sets of specimens in the PB set, slip damage occurred in sets PB1 and PB2, and wire fracture damage occurred in set PB3. The ultimate load of group PB2, in which the relative anchorage length la of the longitudinal wire is 81 mm, is greater than that of group PB1, in which the relative anchorage length is 67.5 mm. When the relative anchorage length la of the longitudinal wire continued to increase to 99 mm, fracture damage occurred in group PB3. With respect to ultimate load, the PB3 group also has a maximum average ultimate load of 15.91 kN, which is greater than the 13.46 kN of the PB2 group and the 12.7 kN of the PB1 group. This demonstrates that increasing the relative anchorage length of the longitudinal wires significantly improves the bonding properties and hence the ultimate load. To verify the above experimental conclusions, the models were built based on the parameters of the PB1 and PB2 specimen groups, respectively, as shown in Figure 12. To reduce the influence of other factors on them, no transverse wire was established in the model and the model was analyzed. As shown in Figure 13, the peak load of the PB2 specimen model was 12.63 kN and that of the PB1 specimen model was 13.23 kN, and the peak load of the PB2 specimen model was significantly higher than that of the PB1 specimen model. It can be seen that the larger the

relative anchorage length, the larger the peak load. This is consistent with the experimental findings, thus verifying the experimental conclusions.

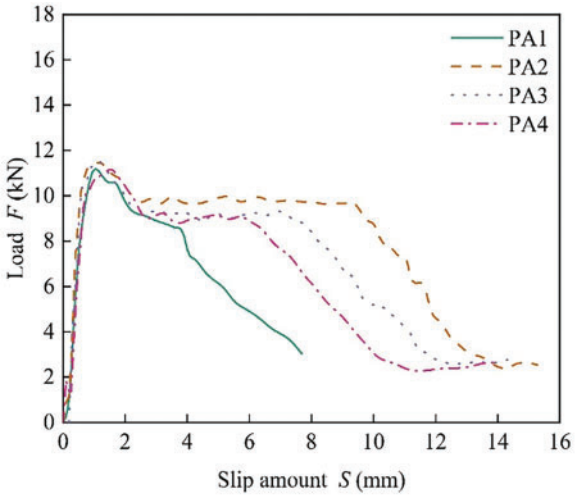

Figure 11. Load-slide curve under PA set

Table 7. Test results under set PB

Specimen set	Specimen set	Ultimate load Fu/kN	Maximum stress τu/MPa	Slip at ultimate load Su/mm	Type of damage
PB1	PB1-1	12.64	13.25	1.11	Slip damage
	PB1-2	12.77	13.39	1.17	Slip damage
	PB1-3	12.69	13.31	1.26	Slip damage
PB2	PB2-1	13.53	11.82	1.47	Slip damage
	PB2-2	13.40	11.71	1.45	Slip damage
	PB2-3	13.46	11.76	1.31	Slip damage
PB3	PB3-1	15.64	–	–	Rupture damage
	PB3-2	16.17	–	–	Rupture damage
	PB3-3	15.92	–	–	Rupture damage

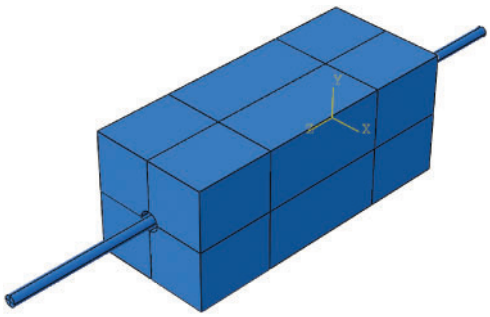

Figure 12. Finite element model of test specimen

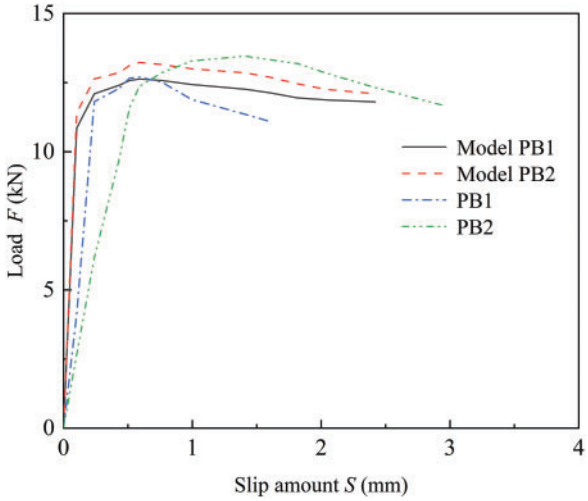

Figure 13. Model load-slip curves for PB1 and PB2 specimens

To further explore the effect of relative anchorage length on peak load. Finite element models with relative anchorage lengths of 5, 10, 15, and 18 d were built and analyzed using ABAQUS, respectively. As shown in Figure 14, the peak loads of the models with relative anchorage lengths of 5, 10, 15, and 18 d are 7.70, 10.11, 12.57, and 13.45 kN, respectively. It can be concluded that the peak loads increase with the increase of the relative anchorage length. The accuracy of the experimental findings is further verified.

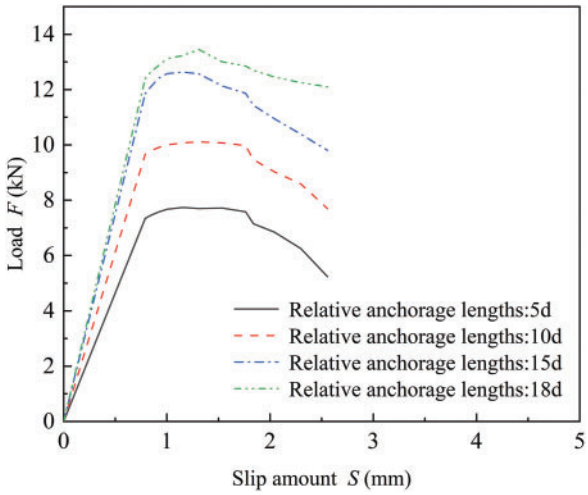

Figure 14. Load-slip curves for models with different relative anchorage lengths

The load-slip relationship curves under the PB specimen set are shown in Figure 15. The PB1 and PB2 groups have similar curve variation patterns, but the PB2 group has a larger ultimate load. After reaching the ultimate load, both sets of curves drop to oscillate around the 11 kN load. As the slip progressively extends to 8 mm, the curve subsequently exhibits a downward trend until the load decreases to 4~5 kN when it enters the smooth section. Eventually, slip damage occurred at 14.67 mm. Unlike PB1 and PB2, the PB3 group has the largest slope right on the upward leg. The slope of the load-slip relationship curve decreases after the load reaches 14 kN, and reaches the transitional point in the curve around 15 kN. Finally, it reaches the average ultimate load at 15.91 kN. The wire fracture damage occurs.

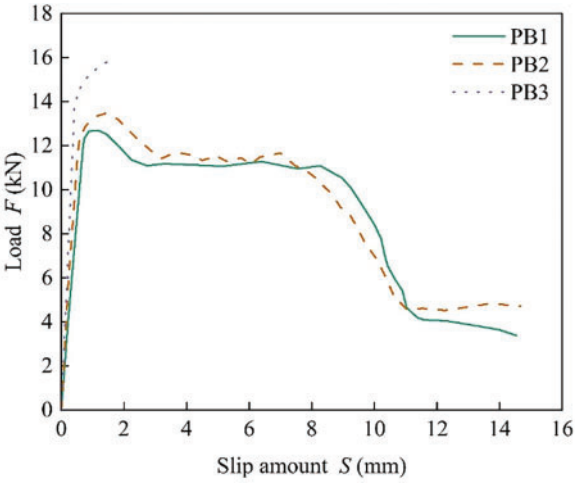

Figure 15. Load-slide curve under PB set

3.1.3 PC specimen set bond anchorage test results

The test results for the PC specimen set are shown in Table 8. Fracture damage occurred in the PC4 group with the longest longitudinal wire relative to the anchorage length la and slip damage occurred in the other specimen groups. Relative to the PB set, the wire diameter d is reduced to 3.2 mm for the PC set. At the same time the relative anchorage length of the longitudinal wire l_a following the same principle as the doubling diameter is also reduced sequentially. The test results showed that the average ultimate load of each specimen group of the PC set at the same multiplication was also reduced relative to that of each specimen group of the PB set after the wire diameter was reduced. However, there is an increase in the maximum stress when the ultimate load is reached. This again verifies this law that the relative anchorage length la of longitudinal wires can influence the bonding properties of the material.

Table 8. Test results under set PC

Specimen set	Specimen set	Ultimate load Fu/kN	Maximum stress τu/MPa	Slip at ultimate load Su/mm	Type of damage
PC1	PC1-1	6.12	15.83	1.16	Slip damage
	PC1-2	6.14	15.91	1.21	Slip damage
	PC1-3	6.09	15.79	1.29	Slip damage
PC2	PC2-1	6.98	14.48	1.31	Slip damage
	PC2-2	7.00	14.51	1.39	Slip damage
	PC2-3	7.07	14.66	1.35	Slip damage
PC3	PC3-1	7.33	12.67	1.56	Slip damage
	PC3-2	7.36	12.72	1.47	Slip damage
	PC3-3	7.44	12.86	1.44	Slip damage
PC4	PC4-1	7.89	–	–	Rupture damage
	PC4-2	8.15	–	–	Rupture damage
	PC4-3	8.02	–	–	Rupture damage

The tensile load-slip curves for the PC specimen set are shown in Figure 16. Similar to the PB set, the load-slip curves of the PC1, PC2, and PC3 groups in the PC set went through the four stages of rising, falling, oscillating (ductile strengthening), and falling again. However, the maximum slip and ultimate load were reduced. Comparing the four specimen sets in this collection, the PC1 set was the first to reach

an average ultimate load of 6.11 kN. It then began to decline and finally slip damage occurred at an average slip of 12 mm. The PC2 and PC3 groups reached the average ultimate load at 7.01 and 7.38 mm, respectively. However, the load-slip curve of the PC3 group was the first to enter the final descending section and finally suffered slip damage at an average slip of 10.78 mm.

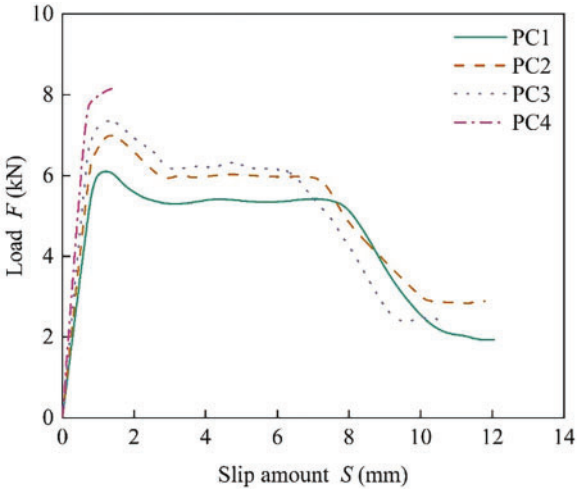

Figure 16. Load-slide curve under PC set

3.1.4 PD specimen set bond anchorage test results

The PD specimen set test results are shown in Table 9. The PD sets all used a 2.4 mm diameter HSSWM. The average ultimate load of each test set under the PD set is further reduced concerning the PC set due to the further reduction in wire diameter. However, the slip of the PD set at ultimate load does not vary much relative to the PA and PC sets. Analogous to the PC4 specimen group, wire fracture damage occurred in the PD4 group with a relative anchorage length l_a of 22 times the diameter. Slip damage occurred in specimen sets of other diameters. Overall, the damage pattern of each specimen group under the PD set is similar to that of the PA and PC sets. It is shown that when the relative anchorage length l_a is high enough, the bond between the two materials is sufficient to pull apart the wire.

Table 9. Test results under set PD

Specimen set	Specimen set	Ultimate load Fu/kN	Maximum stress τu/MPa	Slip at ultimate load Su/mm	Type of damage
PD1	PD1-1	3.55	16.37	1.26	Slip damage
	PD1-2	3.54	16.30	1.33	Slip damage
	PD1-3	3.57	16.45	1.34	Slip damage
PD2	PD2-1	4.11	15.16	1.39	Slip damage
	PD2-2	4.10	15.11	1.48	Slip damage
	PD2-3	4.13	15.24	1.51	Slip damage
PD3	PD3-1	4.27	13.11	1.54	Slip damage
	PD3-2	4.29	13.19	1.64	Slip damage
	PD3-3	4.32	13.26	1.59	Slip damage
PD4	PD4-1	4.42	–	–	Rupture damage
	PD4-2	4.56	–	–	Rupture damage
	PD4-3	4.49	–	–	Rupture damage

The PD specimen set load-slip relationship curve is shown in Figure 17. The PD set though uses a 2.4 mm diameter wire. However, the load-slip relationship curves of its PD1, PD2, and PD3 sets were similar to those of the PA and PC sets of specimens with the same relative anchorage lengths, which also showed four phases of rising, falling, oscillating (ductile strengthening) and falling again. Compared to this, the load-slip relationship curve for the PD4 group rises rapidly at the beginning, and reaches the inflection point of the curve at a load of 4.32 kN, followed by a slow rise. Eventually, the wire fracture damage occurred at an average ultimate load of 4.49 kN.

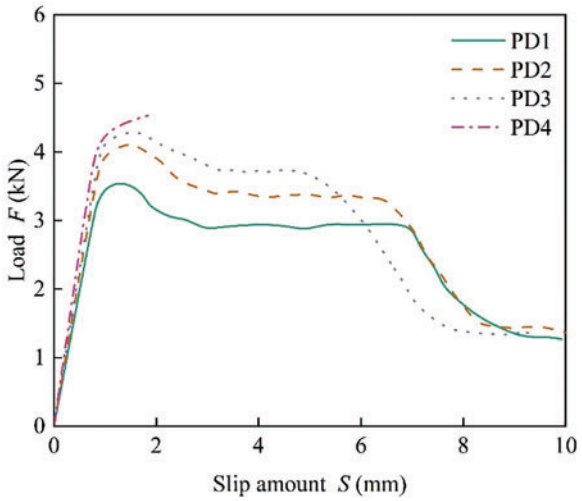

Figure 17. Load-slide curve under PC set

Finite element models were developed using ABAQUS with PB1, PC2, and PD2 specimen parameters to explore the effect of wire diameter on the amount of slip corresponding to peak load. The wire diameters in the models were 2.4, 3.2, and 4.5 mm, which were analyzed separately. As shown in Figure 18, the slip corresponding to the peak load is 1.58, 1.48, and 1.30 mm in the models with wire diameters of 2.4, 3.2, and 4.5 mm, respectively. It can be seen that the slip corresponding to the peak load decreases as the wire diameter increases, which is consistent with the experimental results.

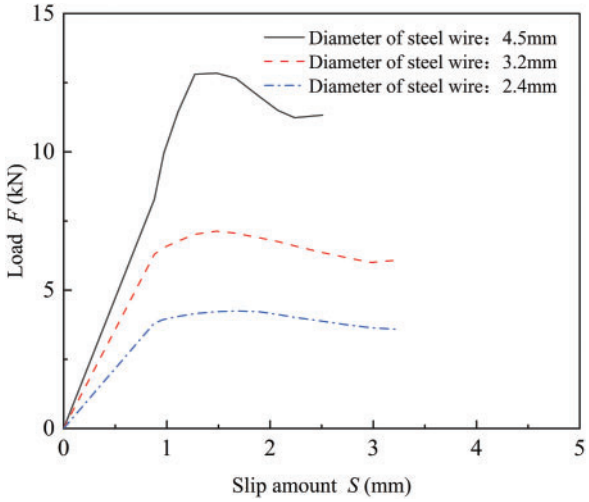

Figure 18. Load-slip curves for models with different wire diameters

3.1.5 PE specimen set bond anchorage test results

Table 10 shows the test results for the PE specimen set. PE set was used with different mixing ratios of PUC to study the effect of glue-to-powder ratio on the bonding properties of HSSWM-PUC composites. Slip damage occurred in the PE1 specimen group, which had a relatively large amount of glue powder, whereas wire breakage damage occurred in the control group, PB2, and in the PE2 group, which had a relatively small amount of glue powder. The PE1 group has the highest average ultimate load of 13.84 kN, greater than the 13.46 kN of the PB2 group and the 13.27 kN recorded for the PE2 group. The damage pattern in this specimen set indicates that the PUC cement powder ratio affects the material bonding properties. The smaller the glue-to-powder ratio under the same conditions, the greater the PUC bond and the easier it is to fracture and damage the wire.

Table 10. Test results under set PE

Specimen set	Specimen set	Ultimate load Fu/kN	Maximum stress τu/MPa	Slip at ultimate load Su/mm	Type of damage
PE1	PE1-1	13.81	10.91	1.23	Slip damage
	PE1-2	14.05	10.87	1.29	Slip damage
	PE1-3	13.69	10.63	1.32	Slip damage
	PE2-1	13.16	–	–	Rupture damage
PE2	PE2-2	13.29	–	–	Rupture damage
	PE2-3	13.35	–	–	Rupture damage

Figure 19 shows the load-slip relationship curves for the specimen groupings PE1, PB2, and PE2. In the rising section of the curve, the PE2 specimen group with the smallest glue-to-powder ratio had the fastest rate of rise. The curve inflection point was reached at a slip of 0.48 mm and rose slowly, and finally, wire fracture damage occurred at 1.43 mm. Relative to the PB2 specimen group with a moderate glue-to-powder ratio, the load-slip relationship of the PE1 specimen group with a larger glue-to-powder ratio decreased rapidly after the shock section. And reached the ultimate slip at 13.81 mm, being less than the 14.67 mm of the PB2 group.

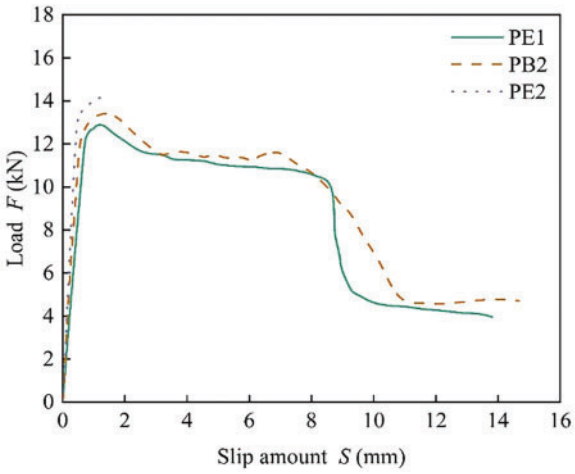

Figure 19. Load-slide curve under PE set

3.2. Analysis of influencing factors

3.2.1 Effect of wire diameter on bonding properties of composites

The relationship between the wire diameter d and the average maximum bond stress is shown in Tables 6–9. As the diameter of the HSSWM increases, the peak average bond stress between the HSSWM and the PUC gradually decreases and the two are negatively correlated. Consider, for example, a specimen with a relative anchorage length of 12 times the diameter. The average maximum bond stress is 16.37 MPa when the wire diameter is 2.4 mm; when the wire diameter is 3.2 mm, the average maximum bond stress is 15.84 MPa; when the wire diameter is 4.5 mm, the average maximum bond stress decreases to 14.47 MPa. The larger diameter wire produces greater radial deformation during stretching, thereby facilitating an increase in the gap. This may be the main reason for the reduction in bond stress.

When the relative anchorage length is constant, the larger the wire diameter is, the smaller the corresponding average slip at the ultimate load. When the relative anchorage lengths were both 12 d, the average slip of the specimen with a diameter of 4.5 mm decreased by about 19% compared with that of the specimen with a diameter of 2.4 mm; when the relative anchorage lengths were 18 d, the average slip of the specimen with a diameter of 4.5 mm decreased by about 11% compared with that of the specimen with a diameter of 2.4 mm. This may be attributed to the larger deformation of the larger diameter wire during tension, resulting in a larger gap between its surface and the PUC, which allows it to reach the peak load quickly, thus reducing the average slip.

3.2.2 Effect of relative anchorage length on bonding properties of composites

The relationship between the relative anchorage la of longitudinal wires and the average maximum bond stress is shown in Tables 6–9. When the wire diameter is constant, the average maximum bond stress decreases gradually as the relative anchorage length increases. Taking the specimen with a diameter of 3.2 mm as an example, when the relative anchorage length is 12 d, the average maximum bond stress is 15.84 MPa; when the relative anchorage length is 15 d, the average maximum bond stress decreases to 14.55 MPa; when the relative anchorage length is 18 d, the average maximum bond stress decreases to 12.75 MPa.

As the relative anchorage length increases, the mean slip at the ultimate load gradually rises and the two are positively correlated. The average slip of the specimen with a wire diameter of 4.5 mm and a relative anchorage length of 18 d was 1.41 mm. This is an improvement of about 19% over the 1.18 mm of the specimen with a relative anchorage length of 15 d; this is an improvement of about 33% over the 1.06 mm of the specimen with a relative anchorage length of 12 d.

3.2.3 Effect of transverse wire spacing on bonding properties of composites

The average slip corresponding to the ultimate load, S_u, and the length of the ductile reinforcement section versus the transverse wire spacing, l_b, are shown in Table 6. As the transverse wire spacing increases, the average slip corresponding to the ultimate load gradually increases. The average slip of the specimens with a transverse wire spacing of 40 mm was 1.39 mm, which was 16% higher than the specimens with a transverse wire spacing of 30 mm and 31% higher than the specimens with a transverse wire spacing of 20 mm. At constant wire diameter and relative anchorage length, the length of the ductile reinforcement section gradually increases as the transverse wire spacing decreases. This indicates that the smaller the spacing of the transverse wires, the stronger their restraining effect on the longitudinal wires.

4. Conclusion

(1) The ultimate load and bond stress pertaining to the composite decreases with increasing wire diameter. Taking the specimen with a relative anchorage length of 12 times the diameter as an example, the average maximum bond stress is 16.37 MPa when the wire diameter is 2.4 mm. The average maximum bond stress is 15.84 MPa when the wire diameter is 3.2 mm. The average maximum bond stress decreased to 14.47 MPa when the wire diameter was 4.5 mm.

(2) As the relative anchorage length increases, the average slip at the ultimate load gradually rises. The wire diameter is 4.5 mm. The average slip of the specimens with a relative anchorage length of 18 d was 1.41 mm. This is an improvement of about 19% over the 1.18 mm of the specimen with a relative anchorage length of 15 d. This is an improvement of about 33% over the 1.06 mm of the specimen with a relative anchorage length of 12 d.

(3) The bond stress-slip curve of the HSSWM-PUC prismatic specimen bond-anchorage test can be divided into four stages, i.e., the rising section, the falling section, the ductile strengthening section, and the residual section. The control group not configured with transverse wires had a shorter ductile reinforcement section, which decreased rapidly after reaching the maximum bond stress. In contrast, the specimen groups formulated with transverse HSSWM had longer ductile reinforcement segments and showed better ductility.

(4) The wire diameter is positively correlated with the length of the ductile reinforcement section, while the relative anchorage length is negatively correlated with the length of the ductile reinforcement section. The ductile properties of HSSWM-PUC composites can be enhanced by increasing the wire diameter.

(5) PUC adhesive powder ratio will affect the bonding properties of composite materials. The slip failure occurred in the test group with a ratio of 1.33 and 1, while the fracture failure occurred in the test group with a ratio of 0.75. This indicates that with an increased cement content, the bonding property of the composite is enhanced. With a higher polyurethane content and a reduced proportion of cement, the bonding property tends to diminish.

Acknowledgement: Not applicable.

References

1. CHEN, B., ZHONG, Z., XIE, X., LU, P., Measurement-based vehicle load model for urban expressway bridges. *Math. Probl. Eng.*, 2014(1), 2014, 340896. https://doi.org/10.1155/2014/340896.
2. LU, P., EASA, S. M., WU, Y., QI, Z., ZHUANG, Y., Hybrid evaluation method of bridge bearing capacity. *Balt. J. Road Bridge Eng.*, 19(3), 2024, 69–101. https://doi.org/10.7250/bjrbe.2024-19.643.
3. ZHAO, J., LI, X., ZHANG, X. C., Experimental and theoretical research on bond performance between CFRP bar and concrete under monotonic and reversed cyclic loading. *Eng. Struct.*, 246(9-10), 2021, 112994. https://doi.org/10.1016/j.engstruct.2021.112994.
4. LUCCIONI, B. M., LÓPEZ, D. E., DANESI, R. F., Bond-slip in reinforced concrete elements. *J. Struct. Eng.*, 131(11), 2005, 1690–1698. https://doi.org/10.1061/(ASCE)0733-9445(2005)131:11(1690).
5. DECÒ, A., FRANGOPOL, D. M., Risk assessment of highway bridges under multiple hazards. *J. Risk Res.*, 14(9), 2011, 1057–1089. https://doi.org/10.1080/13669877.2011.571789.
6. ZHANG, K., XUAN, J., SHEN, X., XUE, X., Investigating the flexural properties of reinforced concrete T—beams strengthened with high-strength steel wire mesh and polyurethane cement. *J. Bridge Eng.*, 29(5), 2024, 04024023. https://doi.org/10.1061/JBENF2.BEENG-6524.
7. YUAN, P., Flexural behavior of reinforced concrete beams strengthened with steel wire mesh and polymer mortar. *Adv. Mater. Res.*, 250, 2011, 1717–1722. https://doi.org/10.4028/www.scientific.net/AMR.250-253.1717.

8. XING, G. H., WU, T., LIU, B. Q., HUANG, X., GU, S. L., Experimental investigation of reinforced concrete T—beams strengthened with steel wire mesh embedded in polymer mortar overlay. *Adv. Struct. Eng.*, 13(1), 2010, 69–79. https://doi.org/10.1260/1369-4332.13.1.69.
9. LI, K., WEI, Y. X., LI, Y. P., LI, Z. Q., ZHU, J. T., Flexural behavior of reinforced concrete beams strengthened with high—strength stainless steel wire rope meshes reinforced ECC. *Constr Build Mater.*, 362(2), 2023, 129627. https://doi.org/10.1016/j.conbuildmat.2022.129627.
10. ZHANG, X. J., FANG, H. Y., DU, M. R., SHI, M. S., ZHANG, C., Experimental study on the mechanical properties of the fiber cement mortar containing polyurethane. *Adv. Mater. Sci.*, 2021(1), 2021, 9956897. https://doi.org/10.1155/2021/9956897.
11. WANG, G. B., FAN, M. T., LIU, Y., Concrete filled steel tubular arch bridge diseases and protective measures. *Adv. Mater. Res.*, 1065–1069, 2015, 930–933. https://doi.org/10.4028/www.scientific.net/AMR.1065-1069.930.
12. AYKAC, S., KALKAN, I., ASCE, A. M., AYKAC, B., KARAHAN, S., et al., Strengthening and repair of reinforced concrete beams using external steel plates. *J. Struct. Eng.*, 139(6), 2013, 929–939. https://doi.org/10.1061/(ASCE)ST.1943-541X.0000714.
13. SALAMA, A. S. D., HAWILEH, R. A., ABDALLA, J. A., Performance of externally strengthened RC beams with side-bonded CFRP sheets. *Compos. Struct.*, 212(6), 2019, 281–290. https://doi.org/10.1016/j.compstruct.2019.01.045.
14. ZHANG, K., SUN, Q., Strengthening of a reinforced concrete bridge with polyurethane—cement composite (PUC). *Open J. Civ. Eng.*, 10(1), 2016, 768–781. https://doi.org/10.2174/1874149501610010768.
15. HUSSAIN, H. K., LIU, G. W., YONG, Y. W., Experimental study to investigate mechanical properties of new material polyurethane-cement composite (PUC). *Constr. Build. Mater.*, 50(5), 2014, 200–208. https://doi.org/10.1016/j.conbuildmat.2013.09.035.
16. YUAN, F., CHEN, M., PAN, J., Flexural strengthening of reinforced concrete beams with high-strength steel wire and engineered cementitious composites. *Constr. Build. Mater.*, 254(1), 2020, 119284. https://doi.org/10.1016/j.conbuildmat.2020.119284.
17. ZHAO, C. Y., HUANG, S. M., YAO, Q. L., CHEN, Y. J., Research on shearing performance of RC beams strengthened with steel wire-polymer mortar. *Appl. Mech. Mater.*, 166, 2012, 1702–1708. https://doi.org/10.4028/www.scientific.net/AMM.166-169.1702.
18. YAN, J., Analysis of common diseases and construction treatment technologies of road and bridge engineering. *Front. Archit. Res.*, 1(2), 2018, 38–42. https://doi.org/10.30564/frae.v1i2.45.
19. QIN, R., ZHOU, A., LAU, D., Effect of reinforcement ratio on the flexural performance of hybrid FRP reinforced concrete beams. *Compos B Eng.*, 108, 2017, 200–209. https://doi.org/10.1016/j.compositesb.2016.09.054.
20. LAU, D., PAM, H. J., Experimental study of hybrid FRP reinforced concrete beams. *Eng. Struct.*, 32(12), 2010, 3857–3865. https://doi.org/10.1016/j.engstruct.2010.08.028.

Received: 05 October 2024; Accepted: 11 June 2025; Published: 18 July 2025